MENTORSHIP, SCHOLARSHIP, AND SERVICE: A SPECIAL ISSUE HONOURING PROFESSOR ADAMU N. BABA-KUTIGI, FNIP ON HIS RETIREMENT
FUDMA Journal of Sciences (FJS)
ISSN online: 2616-1370
ISSN print: 2645 - 2944
Vol. 10 ANB-K Special Issue, 2026, pp 87 – 95
DOI: https://doi.org/10.33003/fjs-2026-10(ANB-K)-5361

Effect of Particle Size on Material Recovery and Elemental Distribution in the Recycling Of End-Of-Life Polycrystalline Silicon Photovoltaic Modules

***[1]Albashir Yasir, [2]S.M Gumel, [1]Waheed Islamiyat O, [1]Tahir Ibrahim D, [1]Ndagi Mohammad, [3]Sule Erten Ela and [4]Hauwa Yahaya Umar**

[1]Department of Pure and Industrial Chemistry, Bayero University, Kano State, Nigeria.
[2]Department of Industrial Chemistry, Federal University, Dutsinma, Dutsinma, Katsina State, Nigeria.
[3]Department of Chemistry, Federal University, Dutsinma, Dutsinma, Katsina State, Nigeria.
[4]Ege University, Solar Energy Institute, Bornova, 35100 Izmir, Turkey.
[5]Department of Chemistry, College of Education (T), Gombe State, Nigeria.

*Corresponding authors' email: ayasir@fudutsinma.edu.ng

ABSTRACT
The rapid deployment of photovoltaic (PV) systems has raised concerns regarding the management of end-of-life (EoL) solar modules. This study investigates the recovery efficiency of polycrystalline silicon PV panels subjected to sequential mechanical and thermal treatments, with emphasis on the influence of particle size distribution on downstream chemical and structural characterization. Disassembled PV modules (≈2 kg per test) were crushed using mortar-and-pestle and hammer-impact methods, followed by sieving into coarse (>5 mm), medium (1–5 mm), and fine (0.08–0.40 mm) fractions. Thermal treatment at 650 °C facilitated the removal of encapsulant materials, after which the recovered fractions were characterized using X-ray diffraction (XRD) and X-ray fluorescence (XRF) analyses. Results indicated improved recovery efficiency in finer fractions, with glass yields increasing from 71.3% in the coarse fraction to 83.4% in the fine fraction. XRD analysis revealed dominant phases of quartz (SiO_2), albite ($NaAlSi_3O_8$), and lime (CaO), while XRF analysis confirmed enrichment of silicon (Si) and antimony (Sb) in finer fractions. Statistical analysis using one-way ANOVA ($p < 0.05$) showed significant differences among particle size fractions in terms of recovery yield and elemental composition, indicating the practical importance of particle size optimization in PV recycling processes. The findings demonstrate that particle size engineering plays a critical role in improving material recovery efficiency and supports the development of sustainable circular photovoltaic recycling strategies.

Keywords: Photovoltaic Waste; Particle Size Distribution; Recycling; XRD; XRF; Circular Photovoltaics; Material Recovery

INTRODUCTION

The rapid expansion of photovoltaic (PV) technology has resulted in unprecedented growth in solar module deployment worldwide. Global PV capacity surpassed 1 TW in 2022 and is projected to exceed 4.5 TW by 2030, leading to a substantial increase in end-of-life (EoL) PV waste generation. Estimates suggest that cumulative PV waste could exceed 78 million tonnes globally by 2050 (International Renewable Energy Agency [IRENA], 2016). Effective management of EoL PV modules is therefore essential for minimizing environmental impacts and supporting circular economy objectives.

Improper disposal of PV modules can result in the loss of valuable materials and the release of hazardous substances such as lead, cadmium, and antimony into the environment. Consequently, recycling has emerged as a critical strategy for sustainable PV waste management, enabling the recovery of valuable materials including glass, silicon, aluminum, silver, and other metals.

Crystalline silicon (c-Si) PV modules, which dominate the global solar market, are primarily composed of glass, aluminum frames, silicon wafers, polymeric encapsulants, and smaller quantities of metallic components (Dias et al., 2016). Various recycling approaches involving mechanical, thermal, and chemical treatments have been developed to recover these materials efficiently (Granata et al., 2014; Pagnanelli et al., 2017). Mechanical pretreatment methods such as hammer and rotor crushing, followed by thermal delamination, have demonstrated effectiveness in improving material liberation and enhancing recovery efficiency (Fiandra et al., 2019).

Despite recent advances in PV recycling technologies, the influence of particle size distribution on material recovery efficiency remains insufficiently investigated. Particle size reduction can improve liberation of embedded materials and enhance downstream recovery processes; however, finer particles may also concentrate hazardous elements and increase handling risks during recycling operations (Kang et al., 2012; Xu et al., 2018). Understanding the relationship between particle size distribution and material recovery is therefore essential for developing efficient and environmentally safe recycling systems.

This study investigates the recovery efficiency of mechanically crushed c-Si PV modules by comparing coarse (>5 mm), medium (1–5 mm), and fine (0.08–0.4 mm) particle fractions obtained after sequential mechanical and thermal treatments. Structural and elemental characterization using X-ray diffraction (XRD) and X-ray fluorescence (XRF) analyses was performed to evaluate the effect of particle size distribution on material composition and recycling efficiency.

MATERIALS AND METHODS

Materials

End-of-life polycrystalline silicon photovoltaic (c-Si PV) modules were used as the input material for this study. Approximately 2 kg of PV module material was processed per experimental run. Prior to treatment, modules were manually

dismantled to remove aluminum frames, junction boxes, and external electrical components.
The following equipment was used during the mechanical pretreatment process:

i. Two-blade rotor crusher
ii. Hammer crusher equipped with a 5 mm sieve
iii. Mortar and pestle
iv. Standard laboratory sieves (8 mm, 5 mm, 1 mm, 0.4 mm, and 0.08 mm)
v. Sample collection bottles

Chemicals
Analytical-grade reagents were used throughout the study:

i. Sulfuric acid (H_2SO_4, 96%, Sigma-Aldrich)
ii. Hydrogen peroxide (H_2O_2, 35% v/v, Sigma-Aldrich)
iii. Deionized water for sample preparation and dilution

Instruments and Analytical Equipment
The following instruments were employed for thermal treatment and material characterization:

i. Resistance furnace (maximum operating temperature: 650 °C)
ii. X-ray diffractometer (XRD, PANalytical X'Pert Pro, Co-Kα radiation, λ = 1.789 Å)
iii. X-ray fluorescence spectrometer (XRF, SPECTRO XEPOS)
iv. Microwave digestion system (Milestone Ethos 900)
v. Atomic Absorption Spectrophotometer (AAS)
vi. Inductively Coupled Plasma Optical Emission Spectrometer (ICP-OES, Varian Vista-MPX CCD simultaneous)

Recycling Procedure
The recycling process consisted of sequential mechanical pretreatment, thermal delamination, chemical digestion, and physicochemical characterization.

Mechanical Pretreatment
The dismantled PV modules were initially fragmented using a two-blade rotor crusher to reduce the module size and facilitate subsequent liberation of encapsulated materials. Secondary crushing was performed using a hammer crusher fitted with a 5 mm sieve.
To ensure reproducibility, each crushing stage was performed under identical operating conditions with three repeated crushing cycles per batch. The crushed material was subsequently sieved into three principal particle size fractions:

i. Coarse fraction: >5 mm
ii. Medium fraction: 1–5 mm
iii. Fine fraction: 0.08–0.4 mm

The fractions were weighed to determine mass distribution and material recovery yield.

Thermal Treatment
Thermal treatment was carried out in a resistance furnace at 650 °C for 1 h under atmospheric air conditions to degrade and remove the ethylene-vinyl acetate (EVA) encapsulant layer binding the PV components.
The furnace heating rate was maintained at 10 °C min^{-1} from ambient temperature to the target temperature. After cooling to room temperature, the thermally treated material was sieved into five size fractions using standard laboratory sieves (8 mm, 5 mm, 1 mm, 0.4 mm, and 0.08 mm). Fractions with particle sizes ≤1 mm were selected for subsequent chemical and structural analyses due to their higher liberation efficiency.

Chemical Digestion
Glass-rich fractions (1–0.08 mm) were subjected to microwave-assisted acid digestion. Approximately 0.2 g of each sample was treated with a mixture of 9 mL concentrated H_2SO_4 (96%) and 1 mL H_2O_2 (35%) in Teflon digestion vessels.
Digestion was performed at 220 °C using a Milestone Ethos 900 microwave digestion system. After digestion, the solutions were cooled, filtered, and diluted with deionized water prior to elemental analysis.
To ensure analytical reliability, all digestion experiments were conducted in triplicate, and blank digestions were included for quality control.

Material Characterization
Mass Balance Analysis
Recovery efficiency was evaluated gravimetrically by measuring the mass distribution of sieved fractions after crushing and thermal treatment.

X-ray Diffraction (XRD)
Crystalline phases present in the recovered materials were identified using a PANalytical X'Pert Pro diffractometer with Co-Kα radiation (λ = 1.789 Å). Data were collected over a 2θ range of 10–80° with a step size of 0.02° and a scanning rate of 2° min^{-1}.

X-ray Fluorescence (XRF)
Elemental composition of the recovered fractions was determined using a SPECTRO XEPOS XRF spectrometer. Measurements were performed on homogenized powdered samples prepared according to the manufacturer's recommendations.

ICP-OES and AAS Analysis
Digested solutions were analyzed for trace metals including Pb, Sb, Ag, and Cd using ICP-OES and AAS techniques. ICP-OES was employed for multi-element quantitative analysis, while AAS was used to validate selected heavy metal concentrations.
Calibration standards and procedural blanks were analyzed alongside samples to ensure measurement accuracy.

Statistical Analysis
All experiments were conducted in triplicate, and results are presented as mean ± standard deviation.
One-way analysis of variance (ANOVA) was used to evaluate the effect of particle size on material recovery efficiency and elemental concentration. Tukey's honestly significant difference (HSD) post-hoc test was applied to compare differences between mean values at a significance level of $\alpha = 0.05$.
Statistical analyses were performed using OriginPro 2023 software.

Table 1: Comparative Summary of Recycling Procedures Adopted for Different Particle Size Fractions

Processing Step	D5 (Coarse Fraction, >5 mm)	D1 (Medium Fraction, 1–5 mm)	D0.08 (Fine Fraction, 0.08–0.4 mm)
Input Material	Polycrystalline silicon PV module (≈2 kg)	Polycrystalline silicon PV module (≈2 kg)	Polycrystalline silicon PV module (≈2 kg)
Manual Disassembly	Removal of aluminum frame, junction box, and external electrical components	Removal of aluminum frame, junction box, and external electrical components	Removal of aluminum frame, junction box, and external electrical components
Primary Crushing	Two-blade rotor crusher	Two-blade rotor crusher	Two-blade rotor crusher
Secondary Crushing	Hammer crusher fitted with 5 mm sieve	Hammer crusher fitted with 5 mm sieve	Hammer crusher fitted with 5 mm sieve
Thermal Treatment	650 °C for 1 h in resistance furnace under atmospheric air	650 °C for 1 h in resistance furnace under atmospheric air	650 °C for 1 h in resistance furnace under atmospheric air
Sieving Procedure	Sieved into 8 mm, 5 mm, 1 mm, 0.4 mm, and 0.08 mm fractions	Sieved into 8 mm, 5 mm, 1 mm, 0.4 mm, and 0.08 mm fractions	Sieved into 8 mm, 5 mm, 1 mm, 0.4 mm, and 0.08 mm fractions
Selected Fraction	Particles >5 mm retained for analysis	Particles between 1–5 mm retained for analysis	Particles between 0.08–0.4 mm retained for analysis
Chemical Digestion	0.2 g sample digested with 9 mL H_2SO_4 (96%) and 1 mL H_2O_2 (35%) at 220 °C using microwave digestion	Same digestion conditions applied	Same digestion conditions applied
Characterization Techniques	XRD, XRF, ICP-OES, and AAS	XRD, XRF, ICP-OES, and AAS	XRD, XRF, ICP-OES, and AAS
Measured Parameters	Mass recovery yield, crystalline phases, and elemental composition	Mass recovery yield, crystalline phases, and elemental composition	Mass recovery yield, crystalline phases, and elemental composition

Note: D5, D1, and D0.08 represent coarse (>5 mm), medium (1–5 mm), and fine (0.08–0.4 mm) particle size fractions obtained after sequential crushing and sieving of polycrystalline silicon photovoltaic modules.

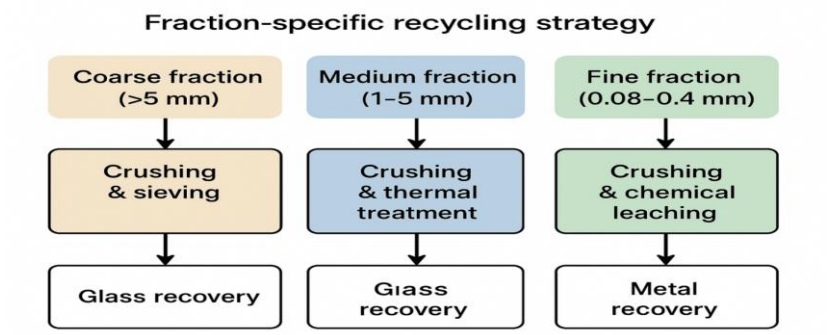

Figure 1: Fraction Specific Recycling Strategy

RESULTS AND DISCUSSION

Effect of Particle Size on Glass Recovery

The effect of particle size on glass-rich fraction recovery after mechanical and thermal treatment is presented in Table 2. Glass recovery increased significantly with decreasing particle size, with the fine fraction (D0.08, 0.08–0.4 mm) exhibiting the highest recovery yield of 83.4 ± 2.4%, followed by the medium fraction (D1, 1–5 mm) at 77.8 ± 1.7%, and the coarse fraction (D5, >5 mm) at 71.3 ± 2.1%.

The observed increase in recovery efficiency with decreasing particle size can be attributed to enhanced liberation of glass particles from encapsulant and metallic components during crushing and sieving operations. Finer fractions exhibited reduced contamination by polymeric residues and improved separation efficiency after thermal delamination.

One-way ANOVA revealed statistically significant differences among the particle size fractions ($F(2,6) = 102.5$, $p < 0.0001$). Tukey's HSD post-hoc analysis confirmed that all pairwise comparisons were statistically significant ($p < 0.001$), indicating that particle size had a strong influence on recovery efficiency.

These findings are consistent with previous studies reporting improved liberation and material recovery at reduced particle sizes during PV recycling processes.

Table 2: Mass Balance and Glass-Rich Fraction Recovery at Different Particle Sizes

Particle Size Fraction	Feed Mass (g)	Mass Recovered (g)	Mass Loss After Furnace (%)	Glass-Rich Fraction Yield (%)
D5 (>5 mm)	2000	1625 ± 30	12.5 ± 0.6	71.3 ± 2.1
D1 (1–5 mm)	2000	1538 ± 25	14.2 ± 0.5	77.8 ± 1.7
D0.08 (0.08–0.4 mm)	2000	1486 ± 28	16.9 ± 0.7	83.4 ± 2.4

Table 3: Tukey's HSD Post-Hoc Comparison of Recovery Yields

Comparison	Mean Difference	p-value	95% CI Lower	95% CI Upper	Significant (α = 0.05)
D5 vs D0.08	+12.07	<0.001	11.53	12.60	Yes
D5 vs D1	+6.50	<0.001	5.97	7.03	Yes
D1 vs D0.08	–5.57	<0.001	–6.10	–5.03	Yes

XRD Analysis of Recovered Fractions

The XRD patterns of the recovered fractions are presented in Figures 3–5. Quartz (SiO_2) and albite ($NaAlSi_3O_8$) were identified as the dominant crystalline phases across all particle size fractions, while minor lime (CaO) peaks were also detected.

The fine fraction (D0.08) exhibited sharper and more intense diffraction peaks compared with the coarse fraction, indicating increased crystallinity and improved liberation of glass-rich phases after crushing and thermal treatment. Minor peaks potentially attributable to Sb-containing phases were also observed in the fine fraction. However, due to the low intensity of these peaks, definitive identification of Sb_2O_3 requires further confirmation using complementary techniques such as SEM-EDS or Rietveld refinement analysis.

The relative phase abundance presented in Table 4 should therefore be regarded as semi-quantitative estimations derived from peak intensity comparison rather than absolute quantitative phase analysis.

Table 4: XRD-Identified Crystalline Phases in Recovered Fractions

Particle Size Fraction	Main Crystalline Phases Detected	Relative Abundance (Semi-Quantitative %)
D5 (>5 mm)	Albite ($NaAlSi_3O_8$), Quartz (SiO_2), Lime (CaO)	Albite 66%, Quartz 23%, Lime 11%
D1 (1–5 mm)	Quartz (SiO_2), Albite ($NaAlSi_3O_8$), Lime (CaO)	Quartz 69%, Albite 20%, Lime 11%
D0.08 (0.08–0.4 mm)	Quartz (SiO_2), Lime (CaO), minor Sb-containing phases	Quartz 74%, Lime 15%, Minor traces

XRF Elemental Composition

The elemental compositions of the recovered fractions determined by XRF analysis are summarized in Table 5. Silicon, calcium, and antimony were identified as the dominant constituents in all particle size fractions, while Pb, Fe, and Ag occurred in lower concentrations.

The concentration of Si increased progressively with decreasing particle size, from 26.8 ± 0.5 wt% in the coarse fraction to 29.9 ± 0.7 wt. % in the fine fraction. This trend indicates enrichment of silica-rich glass phases in finer particles due to enhanced liberation efficiency during crushing.

Similarly, Sb concentration increased slightly in finer fractions, suggesting preferential partitioning of Sb-containing glass additives into smaller particle sizes during mechanical treatment. Trace concentrations of Pb and Ag were also detected, indicating partial retention of metallic impurities within the recovered glass-rich material.

These results agree with previous reports indicating enrichment of heavy metals and glass-forming constituents in fine PV recycling fractions.

Table 5: XRF Major Element Composition of Recovered Fractions

Element (wt. %)	D5 (>5 mm)	D1 (1–5 mm)	D0.08 (0.08–0.4 mm)
Si	26.8 ± 0.5	28.4 ± 0.6	29.9 ± 0.7
Al	1.10 ± 0.04	1.28 ± 0.05	1.36 ± 0.04
Ca	5.35 ± 0.09	5.66 ± 0.08	5.88 ± 0.10
Sb	20.9 ± 0.4	21.5 ± 0.5	22.2 ± 0.5
Fe	0.041 ± 0.002	0.046 ± 0.002	0.050 ± 0.003
Pb	0.022 ± 0.001	0.024 ± 0.001	0.027 ± 0.001
Ag	0.162 ± 0.004	0.171 ± 0.005	0.183 ± 0.006

ICP-OES Analysis of Trace Metals

ICP-OES analysis of digested fractions revealed the presence of trace metals including Pb, Ag, Sb, Cu, and Zn (Table 6). Antimony exhibited the highest concentration among the analyzed metals and increased from 1,850 ± 40 ppm in the coarse fraction to 2,115 ± 55 ppm in the fine fraction.

Lead and silver concentrations also increased with decreasing particle size, indicating progressive enrichment of metallic constituents within finer fractions during crushing and sieving. Cadmium concentrations remained below detectable limits in most fractions, with only trace levels detected in D0.08.

The enrichment of heavy metals in finer fractions highlights the need for controlled handling and safe recycling practices to minimize occupational and environmental exposure risks.

Table 6: ICP-OES Analysis of Trace Metals in Recovered Fractions

Metal (ppm)	D5 (>5 mm)	D1 (1–5 mm)	D0.08 (0.08–0.4 mm)
Cd	<0.05	<0.05	0.08
Pb	92 ± 3	101 ± 4	117 ± 5
Ag	68 ± 2	74 ± 2	81 ± 3
Sb	1850 ± 40	1960 ± 50	2115 ± 55
Cu	11 ± 1	13 ± 1	16 ± 1
Zn	5.1 ± 0.3	5.6 ± 0.3	6.4 ± 0.4

Statistical Evaluation

Statistical analysis confirmed that particle size significantly influenced both recovery efficiency and elemental composition of the recycled fractions ($p < 0.05$). Fine fractions differed significantly from coarse and medium fractions in terms of glass recovery yield and concentrations of Si and Sb.

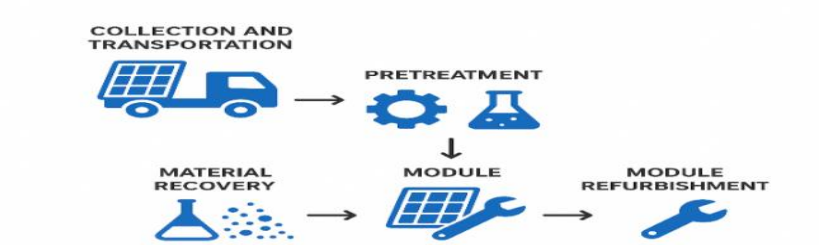

Figure 2: Fraction Obtained After Crushing and Thermal Treatment of Polycrystalline Module

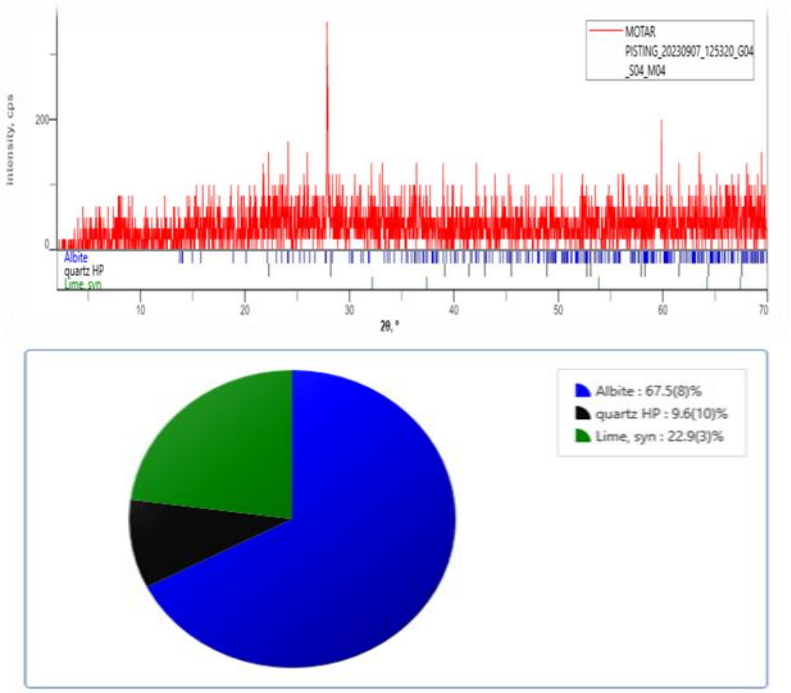

Figure 3: Size Distribution after Treatment of Polycrystalline Module by Mortal Pistol Crushing

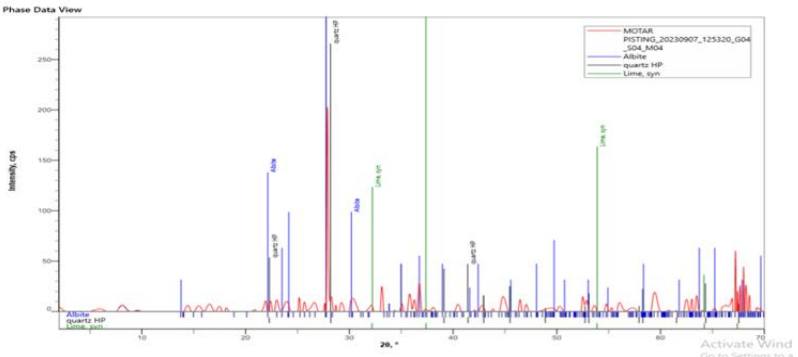

Figure 4: XRD Pattern of Obtained Products after Crushing Plus Hammer Crushin

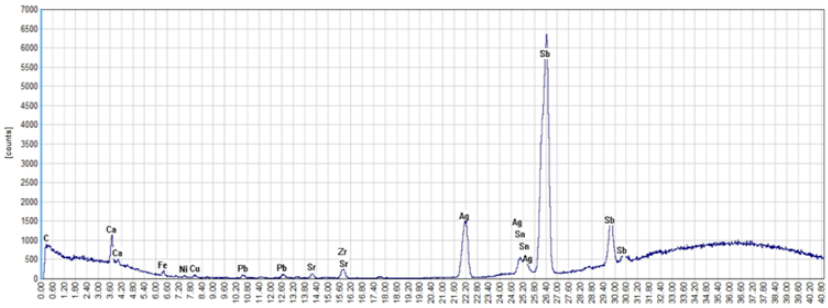

Figure 5: XRD Pattern of Obtained Products after Crushing plus Thermal Treatment

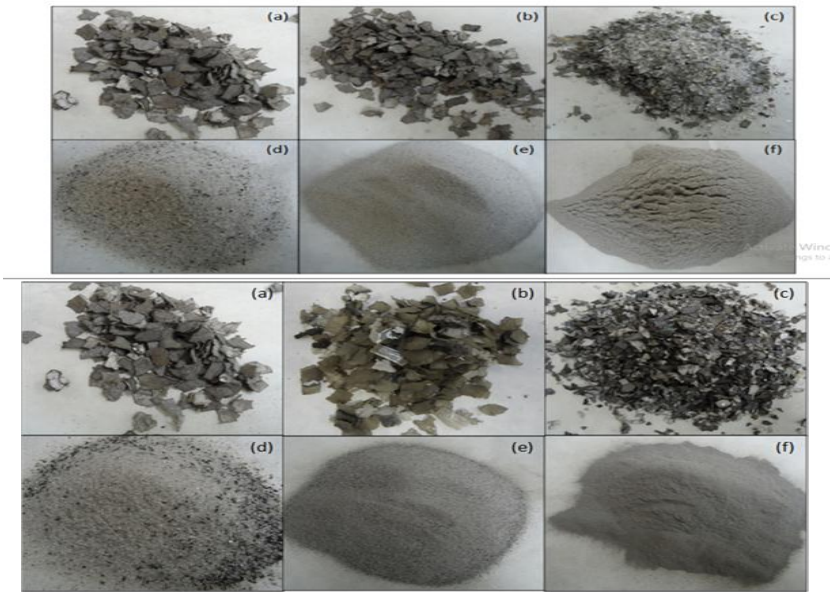

Figure 6: Glass-rich Fractions Obtained after Crushing and Thermal Treatment of Polycrystalline Silicon Photovoltaic (c-Si PV) Modules

Table 7: Semi-Quantitative Phase Distribution Obtained from XRD Analysis

Dataset/Weight Fraction (wt. %)	Albite (%)	Quartz (%)	Lime (%)
Mortar–pestle crushed fraction	67.5 ± 0.8	9.6 ± 1.0	22.9 ± 0.3

Table 8: Representative Peak List from XRD Analysis

No.	2θ (°)	d-spacing (Å)	Peak Height (cps)	FWHM	Intensity (cps)	Crystallite Size (Å)
1	27.842 ± 0.008	3.2017 ± 0.0009	302 ± 49	0.047	24 ± 3	1805 ± 410

Table 9: Phase Identification from XRD Analysis

No.	2θ (°)	Identified Phase	Chemical Formula	PDF Card Number	Profile Type
1	27.842 ± 0.008	Quartz	SiO_2	01-083-0542	Split pseudo-Voigt

Table 10: Qualitative Phase Analysis of Recovered Fractions

Phase Name	Chemical Formula	Figure of Merit	Space Group	Database Card Number
Albite	$NaAlSi_3O_8$	2.770	C-1	00-001-0739
Quartz	SiO_2	0.987	P3121	01-083-0542
Lime	CaO	2.770	Fm-3m	00-004-0777

Discussion

Effect of Particle Size on Mass Recovery and Glass Yield

The results demonstrate that particle size reduction significantly influenced glass recovery efficiency during recycling of polycrystalline silicon photovoltaic (c-Si PV) modules. Fine fractions (0.08–0.4 mm) achieved the highest glass-rich fraction yield (83.4 ± 2.4%), followed by medium fractions (77.8 ± 1.7%) and coarse fractions (71.3 ± 2.1%).

The improved recovery observed in finer fractions is primarily attributed to enhanced liberation of glass particles from EVA encapsulant residues and metallic interlayers during crushing and thermal treatment. Reduction in particle size increases the exposed surface area and weakens bonding between glass and polymeric phases, thereby improving separation efficiency during sieving. Similar liberation-enhanced recovery trends have been reported in previous PV recycling investigations and other comminution-based waste recovery systems.

The higher mass loss observed after furnace treatment in fine fractions may be associated with increased decomposition of residual EVA and volatilization of minor organic components due to the larger reactive surface area of smaller particles. Although fine grinding improved recovery efficiency, additional milling and sieving stages may increase operational energy demand and dust generation in industrial-scale recycling systems. Consequently, the economic benefit of higher recovery must be balanced against processing costs and occupational safety considerations.

Statistical analysis confirmed that particle size had a significant effect on glass recovery efficiency ($F(2,6) = 102.5$, $p < 0.0001$). However, beyond statistical significance, the practical implication is that finer particle production may enhance downstream material purification and critical metal recovery, particularly for glass-rich fractions intended for secondary reuse.

Elemental Distribution and Enrichment Behavior

XRF analysis revealed progressive enrichment of Si and Sb with decreasing particle size. Silicon concentration increased from 26.8 wt% in coarse fractions to 29.9 wt% in fine fractions, while Sb increased from 20.9 wt% to 22.2 wt%.

The increase in Si concentration in fine fractions indicates preferential liberation of silica-rich glass phases during crushing. This trend suggests that mechanical size reduction promotes selective separation of glass components from metallic and polymeric materials. Similar enrichment

behavior has been reported in mechanically treated PV waste, where brittle glass phases preferentially fracture into smaller particles.

The enrichment of Sb and other trace metals such as Pb and Ag in fine fractions is particularly important from both environmental and resource recovery perspectives. Antimony-containing compounds are commonly associated with PV glass additives and flame-retardant materials. During crushing, these phases may preferentially accumulate in finer particles because of differential fracture behavior and increased surface exposure.

Although the observed increase in heavy metal concentration was relatively moderate, fine fractions may represent a potentially hazardous dust stream if improperly handled during large-scale recycling. At the same time, the concentration of valuable metals within these fractions could improve the feasibility of downstream hydrometallurgical recovery processes.

Phase Evolution and XRD Interpretation

XRD analysis identified quartz (SiO_2), albite ($NaAlSi_3O_8$), and lime (CaO) as the dominant crystalline phases across all particle size fractions. Quartz peaks became more prominent in finer fractions, reflecting increased exposure of silica-rich glass material after mechanical liberation.

However, caution should be exercised when interpreting increased peak sharpness as evidence of higher crystallinity. The observed sharpening of diffraction peaks in fine fractions may partially result from particle-size-related diffraction effects and improved sample homogeneity rather than a true increase in crystalline order. Therefore, the XRD results should be interpreted primarily as evidence of enhanced phase exposure and liberation rather than structural crystallization.

Minor Sb-containing phases were detected in fine fractions after thermal treatment. These phases may be associated with oxidation or concentration of antimony-containing additives during milling and furnace treatment. Nevertheless, definitive identification of Sb_2O_3 requires confirmation through complementary analytical techniques such as SEM-EDS, Raman spectroscopy, or Rietveld-refined XRD analysis.

The progressive dominance of quartz in finer fractions indicates that comminution effectively separates brittle glass-rich phases from tougher composite layers within the PV module structure. This observation has practical implications for selective liberation strategies in industrial PV recycling operations.

Heavy Metal Concentration and Environmental Implications

ICP-OES analysis demonstrated progressive enrichment of Pb, Ag, Sb, Cu, and Zn in the finer particle fractions. Lead concentration increased from 92 ppm in coarse fractions to 117 ppm in fine fractions, while Sb exceeded 2,100 ppm in the finest fraction.

This enrichment behavior indicates that fine particles may act as sinks for hazardous and valuable metals during mechanical processing. From a recycling perspective, this concentration effect may be advantageous because it enables targeted recovery of economically important metals from smaller high-grade fractions. Concentrating metals into fine fractions could reduce reagent consumption during subsequent leaching or hydrometallurgical extraction stages.

Conversely, the accumulation of toxic elements in fine powders raises concerns regarding occupational exposure, airborne particulate emissions, and environmental contamination during industrial handling. Fine particulate matter containing Pb and Sb may pose inhalation risks if adequate dust collection and containment systems are not implemented.

Although the present study identified metal enrichment trends, environmental mobility and leachability of these elements were not evaluated. Future studies should therefore include leaching tests such as TCLP or SPLP analysis to assess the environmental behavior of recovered fine fractions under disposal or reuse conditions.

Implications for PV Recycling Process Design

The combined mass balance, XRF, XRD, and ICP-OES results demonstrate that particle size is a critical parameter governing both recovery efficiency and contaminant distribution during PV recycling.

Fine fractions provided the highest glass recovery and greatest enrichment of valuable metals, indicating strong potential for downstream resource recovery. However, the increased concentration of hazardous metals and the likelihood of higher dust generation may complicate industrial handling and environmental management.

Medium-sized fractions (1–5 mm) may therefore represent a practical compromise between liberation efficiency, processing cost, and occupational safety. These fractions achieved relatively high recovery efficiency while potentially minimizing excessive energy consumption associated with ultrafine grinding.

The findings suggest that an optimized PV recycling strategy should adopt fraction-specific processing routes, including:

i. selective grinding to avoid excessive fine dust formation,
ii. targeted hydrometallurgical treatment of fine metal-rich fractions,
iii. controlled thermal delamination for improved liberation efficiency,
iv. And secondary reprocessing of coarse fractions to maximize overall material recovery.

Such an integrated approach could improve the economic and environmental sustainability of crystalline silicon PV recycling systems.

Statistical Interpretation of Particle Size Effects

The one-way ANOVA and Tukey HSD analyses confirmed that particle size reduction significantly influenced glass recovery efficiency and elemental distribution among the recovered fractions.

While statistical significance demonstrates measurable differences between fractions, the practical significance lies in the process engineering implications. The approximately 12% increase in recovery observed between coarse and fine fractions represents a potentially meaningful improvement for industrial recycling systems, particularly when processing large PV waste volumes.

However, the benefits of increased liberation must be balanced against additional grinding energy requirements, dust management costs, and heavy metal concentration in fine fractions. Therefore, optimization of particle size should consider both recovery efficiency and operational sustainability rather than maximizing liberation alone.

CONCLUSION

This study investigated the influence of particle size on the recycling efficiency of end-of-life polycrystalline silicon photovoltaic (c-Si PV) modules using sequential mechanical, thermal, and chemical treatment processes. The results demonstrated that particle size plays a critical role in determining glass recovery efficiency, elemental distribution, and phase liberation during PV recycling.

Fine fractions (0.08–0.4 mm) achieved the highest glass-rich fraction recovery (approximately 83%), confirming that particle size reduction improves liberation of glass and embedded metallic constituents. In contrast, coarse fractions (>5 mm) exhibited lower recovery efficiency due to incomplete separation of encapsulant and composite layers. Elemental analysis further revealed progressive enrichment of Si, Sb, Pb, and Ag in finer fractions, indicating selective concentration of both valuable and hazardous components during crushing and sieving.

XRD analysis identified quartz (SiO_2), albite ($NaAlSi_3O_8$), and lime (CaO) as the dominant crystalline phases in the recovered materials. Minor Sb-containing phases detected in fine fractions suggest that thermal and mechanical treatment can promote concentration of antimony-bearing compounds within smaller particle sizes. ICP-OES analysis confirmed that toxic metals such as Pb and Sb preferentially accumulated in fine powders, highlighting the need for effective dust control and environmentally safe handling during recycling operations.

The findings demonstrate that although fine particle fractions improve recovery efficiency and enhance the potential for critical metal extraction, they also present increased environmental and occupational risks because of heavy metal enrichment. Consequently, an optimized recycling strategy for crystalline silicon PV waste should adopt a fraction-specific approach in which medium-sized fractions (1–5 mm) are prioritized for efficient and safer glass recovery, while fine fractions are subjected to controlled hydrometallurgical or chemical recovery processes for valuable metal extraction.

Overall, this study contributes to the development of sustainable and circular photovoltaic recycling systems by demonstrating how particle size distribution influences both resource recovery and contaminant behavior in end-of-life PV modules. The results provide useful insight for the design of safer and more efficient PV recycling processes aimed at supporting circular economy objectives in the rapidly growing solar energy sector.

Future studies should investigate the leachability and environmental mobility of heavy metals in recovered fractions, as well as the economic feasibility and energy requirements of large-scale particle-size-based PV recycling systems.

REFERENCES

Choi, Y., Shin, H., & Ryu, H. (2017). Recovery of valuable metals from waste silicon solar modules. *Solar Energy Materials and Solar Cells, 162*, 1–7.

Chowdhury, M. S., Rahman, K. S., Chowdhury, T., et al. (2020). An overview of solar photovoltaic panels' end-of-life material recycling. *Energy Strategy Reviews, 27*, 100431.

Clemente, F., Gagliardi, F., et al. (2022). Industrial-scale PV recycling: Technology readiness and economics. *Resources, Conservation and Recycling, 179*, 106075.

Cucchiella, F., D'Adamo, I., & Rosa, P. (2015). End-of-life of used photovoltaic modules: A financial and circular-economy analysis. *Renewable and Sustainable Energy Reviews, 47*, 552–561.

Cucchiella, F., D'Adamo, I., & Terzi, S. (2022). Circular economy of solar photovoltaic panels: An updated review. *Renewable and Sustainable Energy Reviews, 158*, 112152.

Deng, R., Chang, N., Ouyang, Z., & Chong, C. (2019). Recycling of end-of-life crystalline silicon PV modules: Challenges and opportunities. *Renewable and Sustainable Energy Reviews, 109*, 532–550.

Deng, R., et al. (2020). Environmental impacts of crystalline silicon photovoltaic module recycling. *Resources, Conservation and Recycling, 159*, 104854.

Dias, P., Benevit, M., & Veit, H. M. (2020). Advances in silver recovery from photovoltaic waste. *Hydrometallurgy, 191*, 105244.

Dias, P., Javimczik, S., Benevit, M., & Veit, H. M. (2016). Recycling WEEE: Extraction and concentration of silver from waste crystalline silicon photovoltaic modules. *Waste Management, 57*, 220–229.

Fiandra, V., Sannino, L., Andreozzi, C., & Graditi, G. (2019). End-of-life photovoltaic modules recycling: A review of technologies and trends. *Solar Energy Materials and Solar Cells, 201*, 110–123.

Fiandra, V., Bernasconi, R., Turetta, A., et al. (2020). PV module recycling: Comparison of technologies and end-of-life strategies. *Renewable Energy, 149*, 356–365.

Frischknecht, R., Heath, G., Raugei, M., et al. (2020). Life cycle assessment of future photovoltaic electricity production. *Nature Energy, 5*, 868–878.

Granata, G., Pagnanelli, F., Moscardini, E., Havlik, T., & Toro, L. (2014). Recycling of photovoltaic panels by physical operations. *Solar Energy Materials and Solar Cells, 123*, 239–248.

Granata, G., Pagnanelli, F., & Moscardini, E. (2021). Mechanical separation processes for photovoltaic recycling: Case studies. *Separation and Purification Technology, 262*, 118309.

Heath, G., Silverman, T. J., Kempe, M., et al. (2020). Research and development priorities for silicon photovoltaic module recycling to support a circular economy. *Applied Energy, 277*, 115557.

International Energy Agency Photovoltaic Power Systems Programme. (2024). *Advances in photovoltaic module recycling: IEA-PVPS Task 12 report*.

Kang, S., Park, J., Kim, D., et al. (2016). Development of a recycling system for photovoltaic modules. *Solar Energy Materials and Solar Cells, 156*, 1–9.

Kang, S., Yoo, S., & Lee, J. (2012). Experimental investigations for recycling of silicon and glass from waste photovoltaic modules. *Renewable Energy, 47*, 152–159.

Kang, S., Yoo, S., & Lee, J. (2021). Follow-up experimental recycling studies for photovoltaic modules. *Solar Energy Materials and Solar Cells, 221*, 110864.

Klejnowska, K., et al. (2024). Recycling of end-of-life photovoltaic panels: Review of technologies and policy landscape. *E3S Web of Conferences, 475*, 02001.

Latunussa, C. E. L., Ardente, F., Blengini, G. A., & Mancini, L. (2016). Life cycle assessment of an innovative recycling process for crystalline silicon photovoltaic panels. *Solar Energy Materials and Solar Cells, 156*, 101–111.

Lunardi, M. M., Dias, P., Benevit, M., & Veit, H. M. (2018). Assessment of recycling routes for crystalline silicon photovoltaic modules. *Waste Management, 75*, 422–430.

Marwede, M., & Reller, A. (2012). Future recycling flows of tellurium from cadmium telluride photovoltaic waste. *Resources, Conservation and Recycling, 69*, 35–49.

McKenna, R., et al. (2022). Technologies for delamination and polymer recovery from photovoltaic modules. *Journal of Cleaner Production, 330*, 129875.

National Renewable Energy Laboratory. (2021). *solar photovoltaic module recycling: A survey of U.S. policies and practices*.

Nassar, N. T., Dailey, J. N., Olivetti, E. A., et al. (2021). Material criticality and supply risks for photovoltaic component elements. *Nature Materials, 20*, 1231–1241.

Paiano, A. (2022). End-of-life of silicon photovoltaic panels: Trends in recycling technologies. *Journal of Cleaner Production, 359*, 132078.

Paiano, A., et al. (2021). Techno-economic analysis of photovoltaic recycling technologies for glass and metal recovery. *Resources Policy, 74*, 102315.

Pan, P., Benevit, M., & Veit, H. M. (2016). Photovoltaic solar panels of crystalline silicon: Characterization and separation. *Waste Management & Research, 34*(10), 984–992.

Pan, P., et al. (2021). Characterization of recycled photovoltaic glass for secondary applications. *Resources, Conservation and Recycling, 170*, 105588.

Pagnanelli, F., Moscardini, E., Granata, G., et al. (2017). Physical and chemical treatment of end-of-life photovoltaic panels: An integrated process. *Waste Management, 59*, 422–431.

Padhamnath, P. (2025). Recent progress in the recovery and recycling of polymers from end-of-life silicon photovoltaic modules. *Sustainability, 17*(10), 4583.

Preet, S., et al. (2024). A comprehensive review on the recycling technology of photovoltaic panels. *Journal of Cleaner Production, 450*, 141882.

Raugei, M., et al. (2021). Economic and environmental assessment of recycling routes for photovoltaic modules. *Journal of Cleaner Production, 289*, 125728.

Raugei, M., & Fthenakis, V. (2020). Broader resource and climate implications of photovoltaic recycling. *Nature Energy, 5*, 879–880.

Reller, A., & Marwede, M. (2022). Policy drivers and e-waste frameworks for photovoltaic recycling. *Resources Policy, 78*, 102822.

Shen, L., Chen, Z., & Li, N. (2021). Critical review on recycling technologies for crystalline silicon photovoltaic modules. *Journal of Environmental Management, 293*, 112837.

Song, J., Liu, Y., Zhu, H., et al. (2016). Thermal treatment of end-of-life photovoltaic modules: Experimental investigation and environmental assessment. *Journal of Hazardous Materials, 302*, 379–389.

Tao, M., & Fthenakis, V. (2019). Recovery of valuable materials from end-of-life photovoltaic modules. *Progress in Photovoltaics: Research and Applications, 27*, 309–318.

Wambach, K., Libby, C., Shaw, S., & Heath, G. (2024). *Advances in photovoltaic module recycling: IEA-PVPS Task 12 report*. International Energy Agency Photovoltaic Power Systems Programme.

Wei, G., Zhou, Y., Hou, Z., et al. (2025). Review of crystalline silicon photovoltaic module recycling and industrial feasibility. *EES Solar*.

Wilk, G. A., & Potter, W. (2023). Technological trends and emerging processes for photovoltaic waste recycling. *Renewable and Sustainable Energy Reviews, 181*, 113356.

Wilkinson, C., Gaustad, G., & Potter, W. (2024). Antimony in photovoltaic glass: Supply, recycling risk, and processing implications. *Glass Technology: European Journal of Glass Science and Technology Part A, 65*(2), 45–58.

Xu, L., et al. (2025). Antimony material flows and recovery in photovoltaic glass recycling systems. *Journal of Cleaner Production, 512*, 144563.

Yao, Y., Zhu, J., Zhao, J., et al. (2015). Hydrometallurgical processes for recycling spent photovoltaic modules: A review. *Solar Energy Materials and Solar Cells, 132*, 36–45.

Zheng, J., Li, M., & Liu, Q. (2022). Advances in waste photovoltaic module treatment toward sustainable recycling. *Renewable Energy, 192*, 393–405.